*Materials Research*. 2017; 20(Suppl. 2): 317-324
DOI: http://dx.doi.org/10.1590/1980-5373-MR-2016-1062

# Effect of $Fe^{3+}$ Doping in the Photocatalytic Properties of $BaSnO_3$ Perovskite

***Kleber Figueiredo Moura[a], Laís Chantelle[a], Débora Rosendo[a], Elson Longo[b], Ieda Maria Garcia dos Santos[a]****

*[a]Núcleo de Pesquisa e Extensão - NPE, Laboratório de Combustíveis e Materiais - LACOM, Departamento de Química, Universidade Federal da Paraíba, Campus 1, CEP 58059-900, João Pessoa, PB, Brazil.*
*[b]Centro de Desenvolvimento de Materiais Funcionais - CDMF, Laboratório Interdisciplinar de Eletroquímica e Cerâmica - LIEC, Instituto de Química, Universidade Estadual Paulista, Rua Prof. Francisco Degni, 55, Quitandinha, CEP 14800-900, Araraquara, SP, Brazil.*

Received: December 12, 2016; Revised: July 07, 2017; Accepted: July 12, 2017

In the last ten years, stannates with perovskite structure have been tested as photocatalysts. In spite of the ability of perovskite materials to accommodate different cations in its structure, evaluation of doped stannates is not a common task in the photocatalysis area. In this work, $Fe^{3+}$ doped $BaSnO_3$ was synthesized by the modified Pechini method, with calcination between 300 and 800°C/4 h. The powder precursor was characterized by thermogravimetry after partial elimination of carbon. Characterization after the second calcination step was done by X-ray diffraction, Raman spectroscopy and UV-visible spectroscopy. Materials were tested in the photocatalytic discoloration of the Remazol Golden Yellow azo dye under UVC irradiation. Higher photocatalytic efficiency was observed under acid media. As no meaningful adsorption was observed at this condition we believe that an indirect mechanism prevails. $Fe^{3+}$ doping decreased the band gap and favored the photocatalytic reaction, which may be assigned to the formation of intermediate levels inside the band gap.

**Keywords:** *Perovskite, Fe-doped, polymeric precursor method, photocatalysis, RNL.*

## 1. Introduction

Alkaline earth stannates ($MSnO_3$, M = Ba, Sr, Ca) with perovskite structure have become alternative materials to the technological sector due to its applications as dielectric components. Its use as photocatalyst has also been reported, especially for water splitting[1-3] and for the photodegradation of organic dyes, with emphasis in the $SrSnO_3$[4,5]. Previous results of our research group indicated that $BaSnO_3$ has a higher photocatalytic activity than $SrSnO_3$ for the degradation of an azo-dye, the golden yellow remazol (RNL)[6].

$BaSnO_3$ has been studied in various applications in recent years but it is not widely explored as photocatalyst. In spite of its band gap of 3.1 eV, a small activity is usually reported, being assigned to a high electron-hole recombination rate[7]. This drawback may be overcome by the use of nanostructured materials, as reported by Moshtaghi et al.[8,9], who attained a high activity in the photodegradation of organic dyes. A high activity may also be attained, using the perovskite ability to form solid solutions resulting in defects, which can therefore improve its photocatalytic properties[10-12]. For instance, the solid solution $BaSn_{0.2}Pb_{0.8}O_3$ has been evaluated by Borse et al. showing a high activity for the photo-oxidation of water[10]. Literature also reports the use of $La^{3+/2+}$, $Ni^{3+/2+}$, $Fe^{3+/2+}$, $Cu^{2+/+}$, $Co^{3+/2+}$ as dopant into oxides as $TiO_2$, $ZnTiO_3$, $ZnO$[13-17].

$Fe^{3+}$ has been used as $TiO_2$ dopant in several studies[18-23], behaving as electron scavenger which suppress electron-hole recombination improving the photocatalytic efficiency. $Fe^{3+}$ has also been used as $BaSnO_3$ dopant and leads to formation of multi energy levels below the conduction band edge. Charge balance is obtained by formation of oxygen vacancies, besides oxidation or reduction of $Fe^{3+}$, which contribute to the perovskite stabilization[24-26]. The magnetic properties of this Fe-doped perovskite have been studied, but, up to our knowledge, its use as photocatalyst has not been reported yet. The heterogeneous catalysis offers technical and environmental advantages over homogeneous catalysis, allows the recycling of the solid catalyst over its useful life and minimizes the generation of effluents. Several solids have been proposed as potential catalysts for photodegradation of textile dyes. The performance of these materials as catalysts is naturally related to the nature of the acid or basic sites found in these materials.

In the present work, Fe-doped $BaSnO_3$ was synthesized by the modified Pechini method and applied in the photoactivity degradation of RNL azo-dye.

## 2. Experimental

### *2.1 Synthesis of photocatalysts*

$Fe^{3+}$-doped $BaSnO_3$ (0; 0.05 and 0.1 in mol) was synthesized by the modified Pechini method, similarly to the methodology described Lucena et al.[27]. After tin dissolution in a 0.1 $mol.L^{-1}$ nitric acid aqueous solution cooled with an ice bath, citric acid ($C_6H_8O_7.H_2O$, Cargill - 99.5 %) was added into the solution. The pH of the solution was adjusted to 3 by adding ammonium hydroxide ($NH_4OH$, Vetec - 28-30 %). Solutions of iron citrate or barium citrate were prepared from the respective nitrates, $Ba(NO_3)_2$ (Vetec - 99

*e-mail: ieda@quimica.ufpb.br

%), $Fe(NO_3)_3.9H_2O$ (Vetec - 99.5 %), and added into the tin citrate solution under a slow agitation at 25°C for 12 h. A molar ratio citric acid:metal of 3:1 was used for all of the citrates. Ethylene glycol (Vetec - 99.5 %) was added into the solution at 90°C to promote its polymerization. The mass ratio of citric acid to ethylene glycol was 60:40.

The polymeric resins were calcined at 250°C/2 h, deagglomerated, dry milled in a Spex mill, and sieved (100 mesh) to obtain the powder precursors. A heat treatment under an oxygen atmosphere ($O_2$) was performed at a temperature of 300°C /6 h at a heating rate of 1°C $min^{-1}$ under a flow of 1000 $cm^3$ $min^{-1}$ to partially eliminate the organic material. The materials were calcined from 300 to 800°C/4 h under stagnated air atmosphere at a rate of 10°C $min^{-1}$.

The precursors obtained after heat treatment under oxygen atmosphere were characterized by thermogravimetry (TG) and its derivative curve (DTG) using a SDT-2960 thermobalance (TA Instruments) with a heating rate of 10°C $min^{-1}$ up to 1000°C under synthetic air with a flow of 100 mL $min^{-1}$ using alumina crucibles. The samples calcined at 300-800°C were characterized by X-ray diffraction (XRD) using an XRD-6000 Shimadzu diffractometer with Cu Kα radiation between 10° and 80°, using a step size of 0.02° and a step time of 2 s. The values of the lattice parameters were obtained with the Rede93 software using the least squares method. Micro-Raman spectra were obtained in the region of 100-1000 $cm^{-1}$ by an InVia spectrophotometer from Renishaw, using an Ar laser (514 nm) with a power of 20 mW and an objective lens of 50x. UV-vis spectra were obtained by reflectance mode using an UV-2550 Shimadzu spectrophotometer, in the 190-900 nm range.

### *2.2 Photodegradation reaction*

During the photocatalytic test, 15.0 mL of a RNL solution with a concentration of 10 mg $L^{-1}$ and pH = 3 and 6 was placed in a Petri plate with 10 mg of the photocatalyst. The suspensions were irradiated for 1, 2 and 4 h with a Super Niko UVC lamp (0.5-1.0mW), model ZG-30T8. After the reaction, the suspensions were centrifuged at 5000 rpm for 30 min at room temperature before being filtered. The solutions were analyzed by UV-Vis spectroscopy using a SHIMADZU UV-2550 spectrometer, in the range of 300 to 700 nm. The dye discoloration percentage was determined by the measured absorbance at λ = 411 nm, which was assigned to the azo group.

## 3. Results and Discussion

### *3.1 Synthesis and characterization of Fe-doped $BaSnO_3$*

Figure 1 shows the TG and DTG curves of the precursor. Three thermal decomposition steps were observed in the TG curves. In the first step, water and gases adsorbed on the powder surfaces were eliminated; the second step was assigned to the decomposition of the $Ba(NO_3)_2$ between 460 and 680°C; the third step was assigned to the carbonate decomposition[28]. Similar behaviors were obtained by Udawatte et. al.[28] and Li et. al.[29] for the synthesis of $BaSnO_3$ using $BaCO_3$, $SnO_2$ and $BaCl_2$ as precursors.

The X-ray diffraction (XRD) patterns of the materials obtained after heating between 300 and 800 °C are shown in Figure 2.

The planes were indexed according to ICDD 01-074-1300 ($BaSnO_3$), 00-041-1445 ($SnO_2$), 00-045-1471 ($BaCO_3$), 00-024-0053 [$Ba(NO_3)_2$] and 00-0010891 (Sn). For the precursor's heat treated at 300 °C, peaks assigned to tetragonal $SnO_2$, $Ba(NO_3)_2$, Sn and $BaCO_3$ were observed. After heat treatment at 400 °C, higher intensity peaks were observed for $Ba(NO_3)_2$, while the intensities of these peaks decrease at 500 °C. The formation of the cubic $BaSnO_3$ (Pm3m) was observed at 600°C besides a small amount of $SnO_2$ and $BaCO_3$, which is in agreement with the TG/DTG analysis shown in figure 1. This crystallization temperature below 600°C is quite low compared with other synthesis methods as solid state reaction[30-33]. No significant change was observed with temperature increase from 600 to 800 °C.

The XRD patterns of Fe-doped $BaSnO_3$ are shown in Figure 3. Highly crystalline cubic $BaSnO_3$ was observed while no peaks assigned to $Fe_2O_3$ (ICDD 03-065-3107) were found. A slight shift in the diffraction peaks towards higher 2θ values was observed after doping indicating that $Fe^{3+}$ got into $BaSnO_3$ lattice. The lattice parameters, *a*, of $BaSnO_3$ were calculated and indicated that a small lattice decrease took place, which is assigned to the smaller ionic radius of $Fe^{3+}$ (0.64 Å) compared to $Sn^{4+}$ (0.69 Å)[34].

Figure 4 shows the Raman spectra of the $Fe^{3+}$-doped $BaSnO_3$ (0; 0.05 and 0.1 in mol). The group theory predicts the absence of active modes in the Raman spectra for a perfect Pm3m perovskite structure. In spite of this, Cerda et. al.[35] reported bands at 238, 408, 543 and 724 $cm^{-1}$, attributed to distortions of the cubic structure of $BaSnO_3$ due to defects, which modify the internal symmetry of the perovskite phase, leading to unexpected modes in Raman spectra. These modes were assigned to the six fundamental vibrations of $SnO_6$ with $O_h$ symmetry. Similar studies on various perovskite compounds show that distortions of these materials are due to the presence of defects ($V_O^x$, $V'_O$, $V^{\bullet\bullet}_O$,$Sn^{2+}$)[36-38].

Balamuragan et al.[39,40] evaluated the optical and electromagnetic properties of Fe-doped $BaSnO_3$. According to the authors, when iron is added into the perovskite lattice, a center of extrinsic defects is formed with the formation of oxygen vacancies for charge compensation, as showed in Equation (1).

$$Fe_2O_3 \xrightarrow{BaSnO_3} 2Fe'_{Sn} + V_0^{\cdot\cdot} + 3O_0^X \quad (1)$$

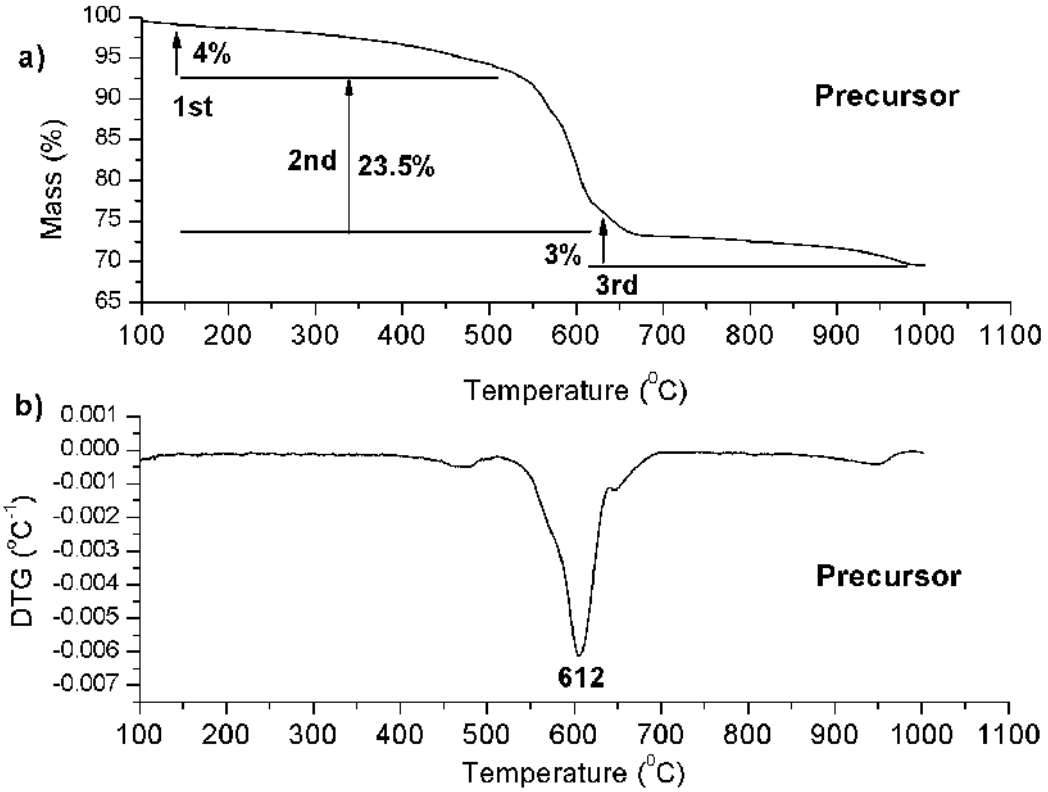


**Figure 1.** a) TG and b) DTG curve of the precursor after heat treatment in the $O_2$ atmosphere at 300°C.

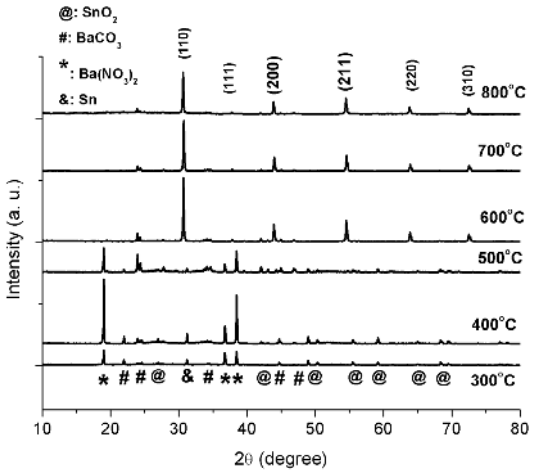


**Figure 2.** XRD patterns of the $BaSnO_3$ heat treated at different temperatures.

In the present work, the mode at 150 $cm^{-1}$ was attributed to the vibration of carbonate groups. Undoped $BaSnO_3$ showed bands at similar regions to those reported by Cerda et al.[35] indicating that distortions are present in the structure. After doping, dislocation of the bands to 252, 413, 535 and 663 $cm^{-1}$ took place. A higher definition was observed for the bands at 252 and 413 $cm^{-1}$, which may be correlated to the oxygen vacancies, which change the symmetry.

Figure 5 shows the absorption spectra of $Fe^{3+}$- doped $BaSnO_3$, with a strong absorption in the visible region. The optical absorption edge of $BaSnO_3$ was observed around 477 nm, with a red shift as doping concentration increases. The band gap values of the as-synthesized samples were estimated from diffuse reflectance spectra using the Wood-Tauc method[41]. Incorporation of $Fe^{3+}$ into the lattice resulted in a band gap decrease, indicating that intermediate levels were formed inside the band gap.

### *3.2 Photocatalytic properties*

The photocatalytic decomposition of RNL by Fe-doped $BaSnO_3$ is presented in Figure 6. The highest degradation efficiency occurred at pH = 3 and the lowest degradation occurred at pH = 6 (aqueous solution of the dye).

Photocatalysis may occur by two different mechanisms: direct or indirect one. For the direct mechanism, dye is adsorbed on the photocatalyst surface and electron transfer takes place without the formation of intermediate compounds. During the indirect mechanism, hydroxyl radicals are formed due to electron/hole transfer between the surface and compounds as $O_2$, $H_2O$ and $OH^-$. Then, hydroxyl radicals in solution react with the substrate.

The possibility of a discoloration by a direct mechanism was evaluated by the adsorption analysis, as adsorption of

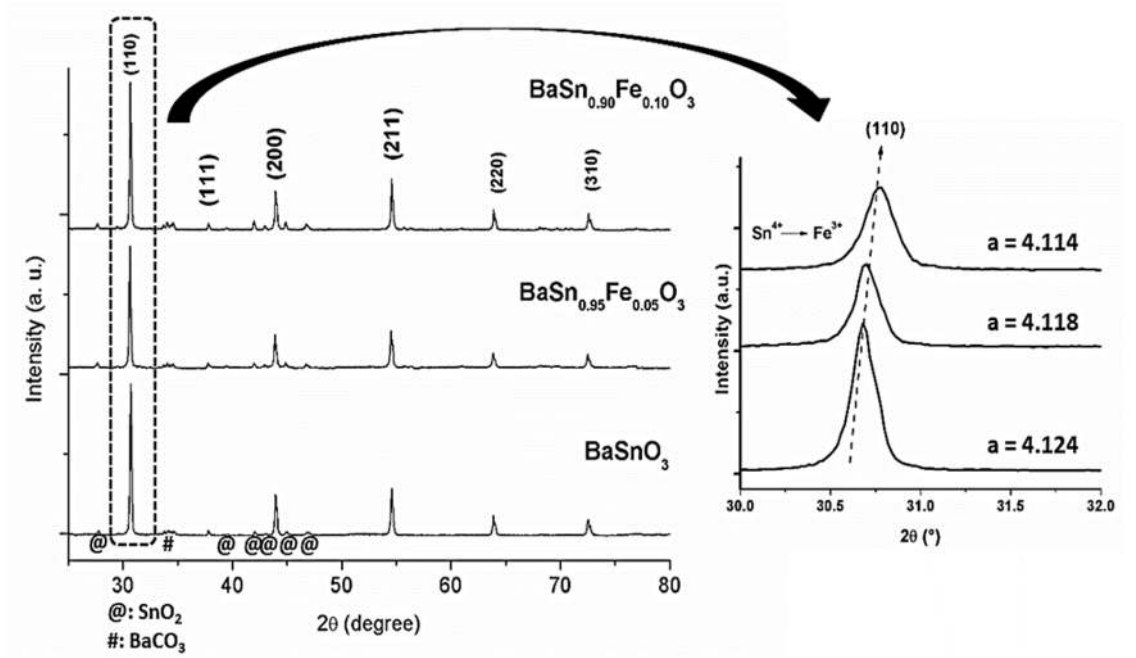


**Figure 3.** XRD patterns of the $BaSn_{1-x}Fe_xO_3$ (0; 0.05 and 0.1 in mol) samples. Detail of the (110) peak in the XRD patterns as a function of the iron concentration.

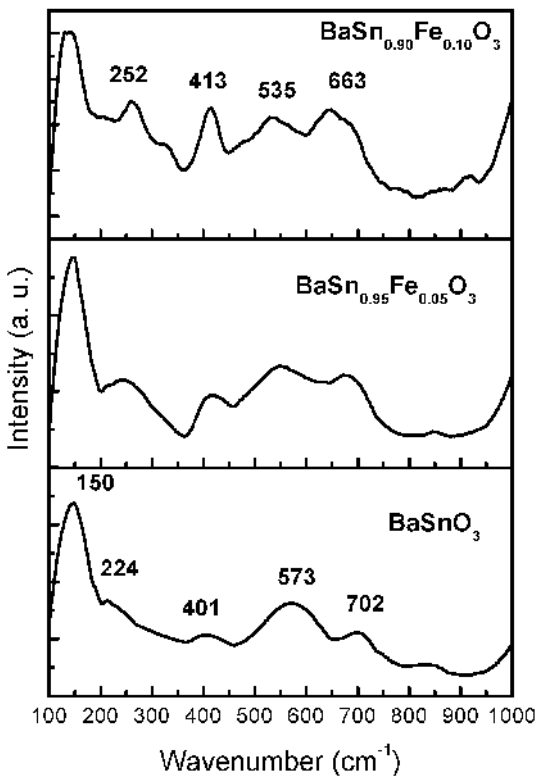


**Figure 4.** Raman spectra of $BaSn_{1-x}Fe_xO_3$ (0; 0.05 and 0.1 in mol) samples.

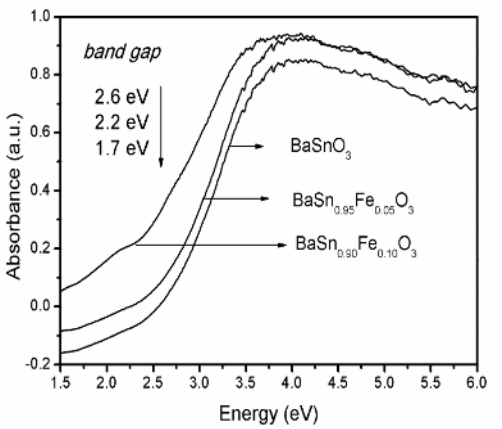


**Figure 5.** UV-Vis spectra of samples $BaSn_{1-x}Fe_xO_3$ (0; 0.05 and 0.1 in mol).

the dye on the material surface is a requested prerequisite step for direct charge transfer[42]. Results displayed in Figure 7 indicate that the maximum discoloration due to adsorption process was 7% for the $BaSn_{0.9}Fe_{0.1}O_3$ sample, much smaller than the discoloration percentage under UVC irradiation (93 %). This small adsorption indicates that the indirect mechanism prevails for this system.

The effect of pH on photocatalysis has been evaluated by different researchers, as reported in the review published by Akpan and Hameed[43]. Much of them report a direct

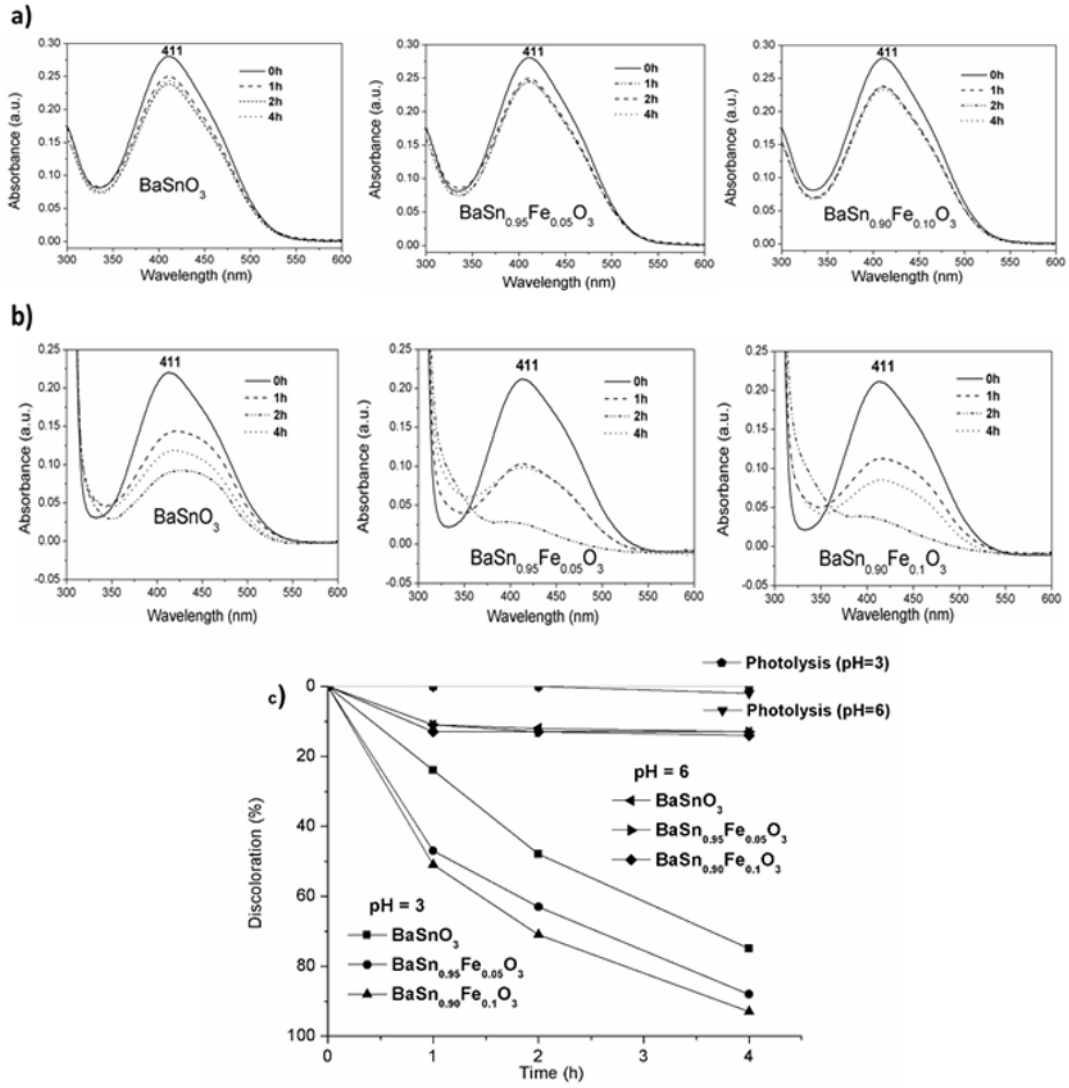


**Figure 6.** Results of the photocatalytic decomposition of RNL as a function of pH for the photocatalysts $BaSn_{1-x}Fe_xO_3$ (x = 0, 0.05 at 0.1 in mol): a) pH = 6; b) pH = 3 and c) Percentage of photodegradation of the RNL.

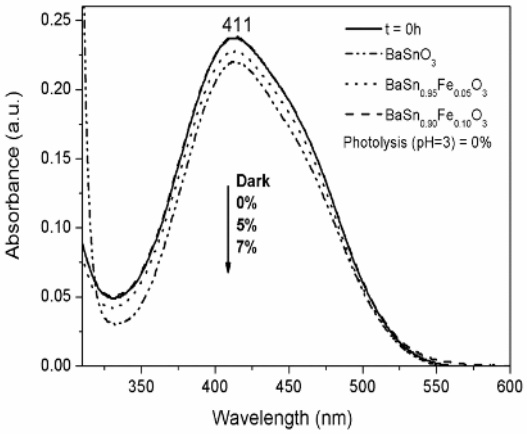


**Figure 7.** Evaluation of RNL adsorption at pH = 3 after 4 h for the samples $BaSn_{1-x}Fe_xO_3$ (x = 0, 0.05 and 0.1 in mol).

mechanism at low pH when $TiO_2$ is used as photocatalyst. On the other hand, according to Guo et al.[44], hydrogen radicals also take part in the photodegradation of phenol using $TiO_2$ as photocatalyst. These $^{\bullet}H$ radicals may be produced from $H_2O$ molecules and also from $H_3O^+$ ions especially in acid media, and may react with $O_2$ forming $HO_2^{\bullet}$ which finally convert to $^{\bullet}OH$. According to Texeira et. al.[45] the RNL azo dye has three $pK_a$ values: the sulphonic group is deprotonated at pH = 3, the sulphate group is deprotonated at pH = 3.5 and the amide group is deprotonated at pH = 6, which results in a large negative charge. Therefore, an attractive force between the positive surface charge of the perovskite and the negative charge of the azo dye occurs at pH 3 favoring the dye attraction and the highest solution discoloration[46]. At pH 6, few molecules are attracted on the $BaSnO_3$ surface due to the slight positive surface charge, leading to a small discoloration of the solution.

In the present work, the highest efficiency at acid media cannot be assigned to a direct mechanism, as only a small adsorption was detected. It seems clear that RNL photodegradation is promoted by $^{\bullet}OH$ radicals whose formation is favored at acidic conditions, probably due to the highest amount of $H_3O^+$ ions.

Figure 6c shows that the color was halved after 1 h of photocatalysis with $BaSn_{1-x}Fe_xO_3$ (x = 0.05 and 0.10), 2.5x higher than undoped $BaSnO_3$. For longer times, doped samples also presented a higher photoactivity than pure one, increasing with Fe content. After 4 h, a photocatalytic efficiency of about 93% was attained for the sample $BaSn_{0.90}Fe_{0.10}O_3$.

Several papers using Fe-doped $TiO_2$ nanoparticles[17-22] assumed that a higher photoactivity for Fe-doped samples is possible in comparison with the undoped material, especially because $Fe^{3+}$ can act as both hole and electron traps to enhance lifetimes of electrons and holes.

Fe-doped $BaSnO_3$ has been studied for magneticelectronics applications, classified as oxide-diluted magnetic semiconductor, displaying ferromagnetism even with small doping amounts. This property is enhanced due to a F-center exchange mechanism, which enables Fe-ions to order ferromagnetically. This F-center is characterized by a $Fe^{n+}$-$V_O$-$Fe^{n+}$ configuration which is able to trap electrons[39,40,47].

In the present work, XRD patterns and Raman spectra indicated that $Fe^{3+}$ was added into the $BaSnO_3$ lattice leading to a shift of the absorption onset to the visible region due to the formation of intermediate levels inside the band gap. These intermediate levels may trap electrons preventing the electron-hole recombination. As a consequence, higher photocatalytic efficiency is obtained.

## 4. Conclusions

$BaSn_{1-x}Fe_xO_3$ (x = 0, 0.05 and 0.10) was successfully synthesized by the modified Pechini method, with crystallization around 600°C. XRD patterns and Raman spectra indicated that $Fe^{3+}$ got into the perovskite lattice leading to a decrease of the band gap. The samples showed high potential for photodegradation of the RNL azo-dye at pH = 3 with prevalence of indirect mechanism. Efficiency was improved by $Fe^{3+}$ doping probably due to the formation of intermediate levels inside the band gap, which may trap electrons avoiding electron-hole recombination.

## 5. Acknowledgements

This work was supported by Brazilian Funding Agencies CT-INFRA/FINEP/MCTIC and CAPES.

## 6. References

1. Omeiri S, Hadjarab B, Bouguelia A, Trari M. Electrical, optical and photoelectrochemical properties of $BaSnO_{3-\delta}$: Applications to hydrogen evolution. *Journal of Alloys and Compounds*. 2010;50(2):592-597.

2. Lee CW, Kim DW, Cho IS, Park S, Shin SS, Seo SW, et al. Simple synthesis and characterization of $SrSnO_3$ nanoparticles with enhanced photocatalytic activity. *International Journal of Hydrogen Energy*. 2012;37(14):10557-10563.

3. Wang W, Bi J, Wu L, Li Z, Fu X. Hydrothermal synthesis and catalytic performances of a new photocalalyst $CaSnO_3$ with microcube morphology. *Scripta Materialia*. 2009;60(3):186-189.

4. Junploy P, Thongtem S, Thongtem T. Photoabsorption and photocatalysis of $SrSnO_3$ produced by a cyclic microwave radiation. *Superlattices and Microstructures*. 2013;57:1-10.

5. Lobo TM, Lebullenger R, Bouquet V, Guilloux-Viry M, Santos IMG, Weber IT. $SrSnO_3$:N - Nitridation and evaluation of photocatalytic activity. *Journal of Alloys and Compounds*. 2015;649:491-494.

6. Sales HB, Bouquet V, Députier S, Ollivier S, Gouttefangeas F, Guilloux-Viry M, et al. $Sr_{1-x}Ba_xSnO_3$ system applied in the photocatalytic discoloration of an azo-dye. *Solid State Sciences*. 2014;28:67-73.

7. Mizoguchi H, Woodward PM, Park CH, Keszler DA. Strong near-infrared luminescence in $BaSnO_3$. *Journal of the American Chemical Society*. 2004;126(31):9796-9800.

8. Moshtaghi S, Zinatloo-Ajabshir S, Salavati-Niasari M. Nanocrystalline barium stannate: facile morphology-controlled preparation, characterization and investigation of optical and photocatalytic properties. *Journal of Materials Science: Materials in Electronics*. 2016; 27(1):834-842.

9. Moshtaghi S, Zinatloo-Ajabshir S, Salavati-Niasari M. Preparation and characterization of $BaSnO_3$ nanostructures via a new simple surfactant-free route. *Journal of Materials Science: Materials in Electronics*. 2016;27(1):425-435.

10. Borse PH, Joshi UA, Ji SM, Jang JS, Lee JS, Jeong ED, et al. Band gap tuning of lead-substituted $BaSnO_3$ for visible light photocatalysis. *Applied Physics Letters*. 2007;90(3):034103.

11. Borse PH, Lee JS, Kim HG. Theoretical band energetics of $Ba(M_{0.5}Sn_{0.5})O_3$ for solar photoactive applications. *Journal of Applied Physics*. 2006;100(12):124915.

12. Yuan Y, Lv J, Jiang X, Li Z, Yu T, Zou Z, et al. Large impact of strontium substitution on photocatalytic water splitting activity of $BaSnO_3$. *Applied Physics Letters*. 2007;91(9):094-107.

13. Weber AS, Grady AM, Koodali RT. Lanthanide modified semiconductor photocatalysts. *Catalysis Science & Technology*. 2012;2(4):683-693.

14. Mostaghni F, Abed Y. Structural, Optical and Photocatalytic Properties of Co-$TiO_2$ Prepared by Sol-Gel Technique. *Materials Research*. 2016;19(4):741-745.

15. Surendar T, Kumar S, Shanker V. Influence of La-doping on phase transformation and photocatalytic properties of $ZnTiO_3$ nanoparticles synthesized via modified sol-gel method. *Physical Chemistry Chemical Physics*. 2014;16(2):728-735.

16. Banić ND, Abramović BF, Šojić DV, Krstić JB, Finčur NL, Bočković IP. Efficiency of neonicotinoids photocatalytic degradation by using annular slurry reactor. *Chemical Engineering Journal* 2016;286:184-190.

17. Pham TD, Lee BK, Lee CH. The advanced removal of benzene from aerosols by photocatalytic oxidation and adsorption of Cu-$TiO_2$/PU under visible light irradiation. *Applied Catalysis B: Environmental*. 2016;182:172-183.

18. Sood S, Umar A, Mehta SK, Kansal SK. Highly effective Fe-doped $TiO_2$ nanoparticles photocatalysts for visible light driven photocatalytic degradation of toxic organic compounds. *Journal of Colloid and Interface Science*. 2015;450:213-223.

19. Garza-Arévalo JI, García-Montes I, Hinojosa Reyes M, Guzmán-Mar JL, Rodríguez-González V, Hinojosa Reyes L. Fe doped $TiO_2$ photocatalyst for the removal of As(III) under visible radiation and its potential application on the treatment of As-contaminated groundwater. *Materials Research Bulletin*. 2016;73:145-152.

20. Ma J, He H, Liu F. Effect of Fe on the photocatalytic removal of NOx over visible light responsive Fe/$TiO_2$ catalysts. *Applied Catalysis B: Environmental*. 2015;179:21-28.

21. Tian F, Wu Z, Tong Y, Wu Z, Cravotto G. Microwave-Assisted Synthesis of Carbon-Based (N, Fe)-Codoped $TiO_2$ for the Photocatalytic Degradation of Formaldehyde. *Nanoscale Research Letters*. 2015;10:360.

22. Li Z, Shen W, He W, Zu X. Effect of Fe-doped $TiO_2$ nanoparticle derived from modified hydrothermal process on the photocatalytic degradation performance on methylene blue. *Journal of Hazardous Materials*. 2008;155(3):590-594.

23. Hemmati Borji S, Nasseri S, Mahvi AH, Nabizadeh R, Javadi AH. Investigation of photocatalytic degradation of phenol by Fe(III)-doped $TiO_2$ and $TiO_2$ nanoparticles. *Journal of Environmental Health Science & Engineering*. 2014;12:101.

24. Vieira FTG, Oliveira ALM, Melo DS, Lima SJG, Longo E, Maia AS, et al. Crystallization study of $SrSnO_3$:Fe. *Journal of Thermal Analysis and Calorimetry*. 2011;106:507-512.

25. Alves MCF, Souza SC, Lima HHS, Nascimento MR, Silva MRS, Espinosa JWM, et al. Influence of the modifier on the short and long-range disorder of stannate perovskites. *Journal of Alloys and Compounds*. 2009;476(1-2):507-512.

26. Lucena GL, Maia AS, Souza AG, Santos IM. Structural changes in Fe-doped $SrSnO_3$ perovskites during thermal analysis. *Journal of Thermal Analysis and Calorimetry*. 2014;115(1):137-144.

27. Lucena GL, Souza JJN, Maia AS, Soledade LEB, Longo E, Souza AG, et al. New methodology for a faster synthesis of $SrSnO_3$ by the modified Pechini method. *Cerâmica*. 2013;59(350):249-253.

28. Udawatte CP, Kakihana M, Yoshimura M. Preparation of pure perovskite-type $BaSnO_3$ powders by the polymerized complex method at reduced temperature. *Solid State Ionics*. 1998;108(1-4):23-30.

29. Li B, Tang Y, Luo L, Xiao T, Li D, Hu X, et al. Fabrication of porous BaSnO3 hollow architectures using $BaCO_3$@$SnO_2$ core-shell nanorods as precursors. *Applied Surface Science*. 2010;257(1):197-202.

30. Huang C, Wang X, Liu X, Tian M, Zhang T. Extensive analysis of the formation mechanism of $BaSnO_3$ by solid-state reaction between BaCO3 and SnO2. *Journal of the European Ceramic Society*. 2016;36(3):583-592.

31. Manju MR, Kumar VP, Dayal V. Investigation of ferromagnetic properties in Fe/Co substituted $BaSnO_3$ perovskite stannates. *Physica B: Condensed Matter*. 2016;500:14-19.

32. Ochoa YH, Schipani F, Aldao CM, Ponce MA, Savu R, Rodríguez-Páez JE. Electrical behavior of $BaSnO_3$ bulk samples formed by slip casting: Effect of synthesis methods used for obtaining the ceramic powders. *Materials Research Bulletin*. 2016;78:172-178.

33. Kumar AA, Kumar A, Quamara JK, Dillip GR, Joo SW, Kumar J. Fe (III) induced structural, optical, and dielectric behavior of cetyltrimethyl ammonium bromide stabilized strontium stannate nanoparticles synthesized by a facile wet chemistry route. *RSC Advances*. 2015;5:17202-17209.

34. Balamurugan K, Kumar ES, Ramachandran B, Venkatesh S, Kumar NH, Rao MS, et al. Dielectric resonance and magnetic properties of Fe-3% doped $BaSnO_3$ thin films grown by pulsed laser deposition. *Journal of Applied Physics*. 2012;11(7)074107.

35. Cerdà J, Arbiol J, Diaz R, Dezanneau G, Morante JR. Synthesis of perovskite-type $BaSnO_3$ particles obtained by a new simple wet chemical route based on a sol-gel process. *Materials Letters*. 2002;56(3):131-136.

36. Stanislavchuk TN, Sirenko AA, Litvinchuk AP, Luo X, Cheong SW. Electronic band structure and optical phonons of $BaSnO_3$ and $Ba_{0.97}La_{0.03}SnO_3$ single crystals: Theory and experiment. *Journal of Applied Physics*. 2012;112(4):044108.

37. Zhang W, Tang J, Ye J. Structural, photocatalytic, and photophysical properties of perovskite $MSnO_3$ (M = Ca, Sr, and Ba) photocatalysts. *Journal of Materials Research*. 2007;22(7):1859-1871.

38. Zheng H, de Györgyfalva GDCC, Quimby R, Bagshaw H, Ubic R, Reaney IM, et al. Raman spectroscopy of B-site order-disorder in $CaTiO_3$-based microwave ceramics. *Journal of the European Ceramic Society*. 2003;23(14):2653-2659.

39. Balamurugan K, Harishn Kumar N, Arout Chelvane J, Santhosh PN. Room temperature ferromagnetism in Fe-doped $BaSnO_3$. *Journal of Alloys and Compounds*. 2009;472(1-2):9-12.

40. Balamurugan K, Harish Kumar N, Arout Chelvane J, Santhosh PN. Effect of W co-doping on the optical, magnetic and electrical properties of Fe-doped $BaSnO_3$. *Physica B: Condensed Matter*. 2012;407(13):2519-2523.

41. Wood DL, Tauc J. Weak Absorption Tails in Amorphous Semiconductors. *Physical Review B*. 1972;5(8):3144-3151.

42. Tang WZ, Huang CP. Photocatalyzed oxidation pathways of 2,4-dichlorophenol by CdS in basic and acidic aqueous solutions. *Water Research*. 1995;29(2):745-756.

43. Akpan UG, Hameed BH. Parameters affecting the photocatalytic degradation of dyes using $TiO_2$-based photocatalysts: A review. *Journal of Hazardous Materials*. 2009;170(2-3):520-529.

44. Guo Z, Ma R, Li G. Degradation of phenol by nanomaterial $TiO_2$ in wastewater. *Chemical Engineering Journal*. 2006;119(1):55-59.

45. Teixeira TPF. *Avaliação da eficiência do uso de hidrotalcitas calcinadas na remoção de azo corantes aniônicos presentes em efluentes de indústria têxtil*. Dissertation. Ouro Preto: Universidade Federal de Ouro Preto; 2011. 93 f.

46. Teixeira TPF, Pereira SI, Aquino SF, Dias A. Use of Calcined Layered Double Hydroxides for Decolorization of Azo Dye Solutions: Equilibrium, Kinetics, and Recycling Studies. *Environmental Engineering Science*. 2012;29(7):685-692.

47. Swatsitang E, Karaphun A, Phokha S, Putjuso T. Characterization and magnetic properties of $BaSn_{1-x}Fe_xO_3$ nanoparticles prepared by a modified sol-gel method. *Journal of Sol-Gel Science and Technology*. 2016;77(1):78-84.